Journal of Solid State Chemistry 188 (2012) 50–58

Contents lists available at SciVerse ScienceDirect

Journal of Solid State Chemistry

journal homepage: www.elsevier.com/locate/jssc

Ultra fast elemental synthesis of high yield copper Chevrel phase with high electrochemical performance

Gregory Gershinsky, Ortal Haik, Gregory Salitra, Judith Grinblat, Elena Levi, Gilbert Daniel Nessim, Ella Zinigrad, Doron Aurbach *

Department of Chemistry, Bar-Ilan University, Ramat-Gan, 52900, Israel

ARTICLE INFO

Article history:
Received 4 October 2011
Received in revised form
2 January 2012
Accepted 9 January 2012
Available online 2 February 2012

Keywords:
Chevrel phases
Cluster compounds
Self-propagating high-temperature synthesis
Combustion
Phase diagram

ABSTRACT

Self-propagating High-temperature Synthesis (SHS) was applied for the first time to prepare Chevrel phases, $M_xMo_6T_8$ (M=metal, T=S, Se). Combined electron microscopy and X-ray powder diffraction were used to clarify the chemical reactions in the Cu–Mo–S system. It was shown that the replacement of the frontal combustion by thermal explosion increased the $Cu_2Mo_6S_8$ yield from 86 to 96%, while the synthesis remained ultra-fast: 10–20 min in a hot furnace (1000 °C), as compared to at least 17 h of heating for the conventional solid state technique. The synthesized material conformed to the requirements of cathode precursors for Mg batteries, and its electrochemically activity was similar to that of the conventional product.

1. Introduction

The molybdenum chalcogenides, $M_xMo_6T_8$ (M=metal, T=S, Se, Te), also known as Chevrel phases, are an important class of inorganic compounds with remarkable superconductive, magnetic, thermoelectric, and catalytic properties [1–4]. Their crystal structure is based on the Mo_6-clusters, octahedral groups of molybdenum atoms with metal–metal bonds [1, 2]. Our interest in Chevrel phases is related to their unusually high cation mobility at ambient temperatures [5], which allows using the sulfides and selenides as unique cathodes in "green" Mg rechargeable batteries [6, 7], or as ceramic membranes for selective cation extraction from liquid wastes [8].

Two major ways to produce Chevrel phases were proposed. The first method is a high-temperature solid state synthesis, first reported by Chevrel et al. [9], where a stoichiometric mixture of the elements or chalcogenides is sealed under vacuum in a quartz ampoule, and heated over several days at temperatures reaching 1100–1200 °C. Although it was shown that Chevrel phases can be prepared at much lower temperatures [10], the long annealing at ~1100 °C is necessary to reduce the amount of undesirable impurity, layered MoT_2 [11]. In the second approach reported by Rabiller-Baudry et al. [12], Chevrel phases were synthesized from soluble sulfide precursors, such as polythiomolybdates and metal salts, by multi-step heating up to 800 °C. This method generated particles with high surface area, crucial for catalysis, but presented two major disadvantages: (1) the polythiomolybdates themselves had to be pre-synthesized and (2) the hydrogen flow used as a reducing agent in the reaction had to be strictly controlled.

In order to reduce the duration and the temperature of the solid-state synthesis, in our previous work we proposed using stainless-steel Swagelok tube fittings [13] instead of the quartz ampoule, or performing the synthesis in a molten salt media (KCl) [14]. A great advantage of the last method is its suitability for mass-production of Chevrel phases (Table 1), but still the synthesis takes days and requires special equipment with high-energy consumption. These drawbacks can be overcome by using self-propagating high-temperature synthesis (SHS), a relatively novel and simple technique [15–19]. The main principle of SHS is to initiate a self-sustaining highly exothermic reaction in the form of a combustion wave or thermal explosion. The temperatures reached are extremely high (up to 4000 K) and the burning front propagates at high speed (between 0.1 and 20 cm/s) [19]. The synthesis is extremely fast and the overall reaction process takes only a few seconds or minutes. The material obtained with SHS usually presents high porosity, which may be regarded as an advantage for electrochemical and catalytic applications.

A selection of reactions suitable for SHS is commonly based on thermodynamic calculations, in particular on the adiabatic flame

* Corresponding author. Fax: +97237384053.
E-mail address: Doron.Aurbach@biu.ac.il (D. Aurbach).

0022-4596/$ - see front matter © 2012 Elsevier Inc. All rights reserved.
doi:10.1016/j.jssc.2012.01.016

Table 1
Comparison of the energy consumption parameters for different methods of the solid-state synthesis of Chevrel phase, $Cu_2Mo_6S_8$.

Method	Temprature of synthesis T_s,°C	Time		Potencial of larga scaling	Ref.
		Heating from RT to T_s (h)	Dwelling at T_s		
Cinventional solid state synthesis in quartz tube	1050	48	48 h	No	[27]
Cinventional solid state synthesis in Swagelock	900	8	16 h	Yes	[13]
Synthesis in molten salt	850	6	60 h	Already industrial	[14]
Thermal explosion or bulk mode of SHS	1000	–	10–20 min	Yes	This work

temperature T_{ad} that should be higher than 1800 K. The calculations by Goroshin et al. [20] showed that the combustion should be sufficient to synthesize most of the binary metal–sulfur mixtures. Based on the known high release of heat for the metal–chalcogen reactions, it is expected that the SHS method should be convenient for the Chevrel phase production. Two additional points appear to favor the combustion synthesis of $M_xMo_6T_8$:

- The high thermal conductivity of the starting ternary mixtures, which is related to the large metal/chalcogenide ratio in its composition, should lead to fast heat transmission from the hot to the cold layers.
- The low thermal conductivity of Chevrel phases [3] should result in the slow heat loss in the after-burning zone, thus leading to a more complete reaction.

However, the technical simplicity of SHS is associated with a complexity of physico–chemical processes, which take place upon combustion and subsequent crystallization of the synthetic products. In addition, the extreme character of the combustion reactions results in the intrinsic difficulties of their studies. As a result, practical use of this method for chalcogenides was mostly restricted to binary systems [20–23]. Since little is known about the mechanism of the ternary reactions, the ability of any three-component mixture to produce a stable combustion wave should be verified in practice.

Thus, the aim of this work is to study the potential of SHS for synthesizing Chevrel phases. It is shown that five interesting compounds (Mo_6Se_8, $MnMo_6S_8$, $Cu_2Mo_6S_8$, $PbMo_6S_8$ and $PbMo_6Se_8$) can be obtained by combustion (to our knowledge, we are the first to present the SHS of cluster compounds). However, from the relatively low product yields obtained in these preliminary experiments, it was clear that each M–Mo–T system requires individual optimization of synthetic parameters like particle size of reactants, composition of the green mixture, combustion atmosphere and pressure, initial temperature and so on. We focus herein on the formation mechanism for $Cu_2Mo_6S_8$, as the best precursor for the Mo_6S_8-based cathodes in rechargeable Mg batteries. The phase relations in the Cu–Mo–S system were studied by combined X-ray powder diffraction, electron microscopy and thermal analysis. Based on this study, the bulk mode of SHS (thermal explosion) is further proposed. The electrochemistry of the material with high yield of $Cu_2Mo_6S_8$ obtained by combustion is compared with that of Chevrel phase produced by conventional long-term solid-state synthesis.

2. Experimental

2.1. Materials

The combustion products were obtained from the elemental high-purity powders (Aldrich: 99.95% for Mo < 10 μm; 99.9% for Mo < 5 μm; 99.98% for S; 99.7% for Cu < 10 μm; 99.5% for Cu < 20 μm; 99.99% for Mn; 99.95% for Pb; Acros: 99.7% for Se) mixed in stoichiometric proportions. The green mixture was ground in a mortar and pestle for ~2 min, pressed into a pellet (pressure of 0.134 GPa) and then ground again. This procedure was repeated twice. For the Mn–Mo–S system, in addition to elements, a mixture of MnS (99.9%, Aldrich), molybdenum and sulfur was tested. For the Cu–Mo–S system we also used composition of $Cu_2Mo_6S_{8.5}$ with extra sulfur amount. The morphology of the Cu and Mo precursors can be seen from the SEM images in Fig. 1. The particle size for other precursors was 2–15 μm for Pb, 8–35 μm for Mn and 1–2 μm for MnS.

2.2. Synthetic methods

We initiated the combustion reaction using two distinctive techniques:

- Frontal combustion (for all the M–Mo–T systems under study): The combustion was performed in quartz tubes under Ar (Fig. 2) or vacuum (for the Mn–Mo–S system). The ratio between reactants (about 10 g) and total reactor volume was 1 to 10. The reactions were initiated at the bottom part of the tube by temperature controlled furnace heated up to 800 °C, which can be considered as the onset temperature for initiation of the reaction, or by applying propane–oxygen Bunsen burner at 1500 °C to the reaction tube for a period of less than a second.
- Thermal explosion or bulk combustion (for the Cu–Mo–S system): The elemental mixture (2 or 5 g) with extra sulfur ($Cu_2Mo_6S_{8.5}$ stoichiometry) was loaded into a Swagelok stainless steel vessel under argon atmosphere, and introduced in the hot furnace (1000 °C) for 2 and 10 min for 2 g samples or for 10 and 20 min for 5 g samples. The ratio between reactant and total reactor volumes was 1 to 2.

Each experiment was repeated at least twice with similar results.

For the X-ray diffraction analysis (XRD) the Cu–Mo–S elemental mixture was loaded into stainless steel Swagelok under argon atmosphere and heated at a rate 1 °C/min in a furnace to different temperatures, without annealing and for 24 h of annealing. For comparative purposes, $Cu_2Mo_6S_8$ was prepared also by a known [13] solid-state technique: a mixture of binary sulfides (MoS_2, CuS) and elemental Mo loaded in Swagelok was heated at a rate 0.75 °C/min in a furnace to 900 °C, for 17 h annealing.

2.3. Electron microscopy, X-ray diffraction and thermal analysis

Scanning electron microscopy of the materials was carried out with a FEI Inspect-S SEM operating at 15 kV. Surface area measurements were calculated according to the B.E.T model.

High-resolution transmission electron microscopy was carried out with a JEOL JEM-2100 LaB_6 at 200 kV. Transmission Electron

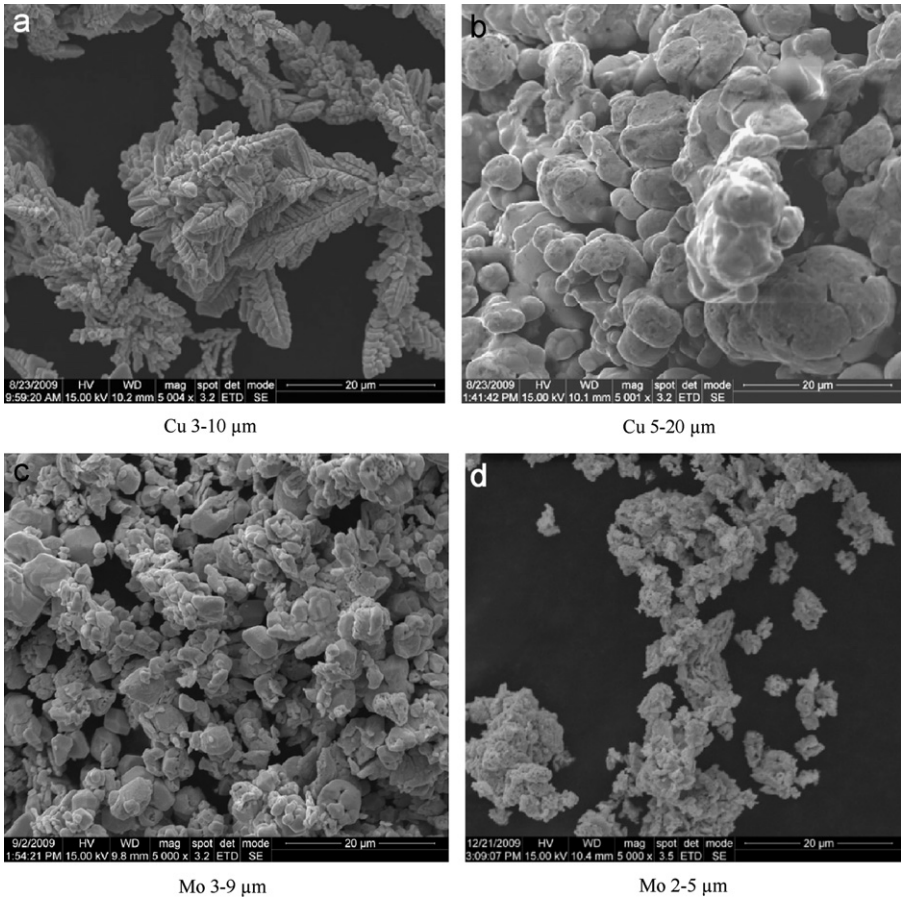

Fig. 1. Scanning electron microscopy images of copper and molybdenum powder: (a) Cu 3–10 μm, (b) Cu 5–20 μm, (c) Mo 3–9 μm, (d) Mo 2–5 μm.

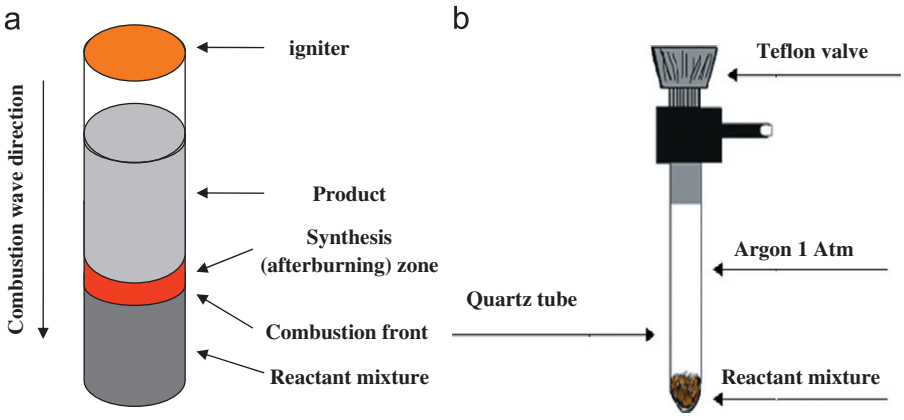

Fig. 2. Schematic diagram of the combustion process (a) and quartz reactor scheme (frontal mode) (b).

Microscope (TEM) and High Resolution Transmission Electron Microscope (HRTEM) studies were performed in order to provide supporting evidence for the morphology, elemental content and structure of the reaction product at 450 °C. These studies were performed in TEM mode, using conventional selected area electron diffraction (SAED) technique, nano-beam diffraction (NBD) or Fourier transform analysis (FFT) of the high-resolution images. The characterization and identification of the resulting nanoparticles was further supported by elemental analysis techniques, such as, Energy dispersive X-ray spectroscopy (point EDS).

X-ray diffraction (XRD) studies were performed with a Bruker Inc. (Germany) AXS D8 ADVANCE diffractometer (reflection θ–θ geometry; Cu $K\alpha$ radiation, Ni-filter; scintillation counter). Rietveld method based on the FULLPROF program [24, 25] was used for the quantitative phase analysis. The divergence, anti-scattering and receiving slits are 0.6, 0.3 and 0.2 mm, respectively. Diffraction data were collected in the angular range of $10^\circ < 2\theta < 110$–140°, step size 0.02°, step time 10–30 s/step. Thompson–Cox–Hastings pseudo-Voigt functions were used for the peak-shape approximation. The background was refined by a polynomial function or linear interpolation between background points. The agreement factors used in this article are defined according to the guidelines of the Rietveld refinement that can be found elsewhere [26].

Multiple Module Calorimeter (MMC) Model 274 Nexus from NETZSCH was used for thermal analysis. MMC measurements were conducted in hermetically sealed standard titanium tubes, 6 ml in volume, over a temperature range of 40–450 °C. The tubes were filled with about 400 mg of the elemental powder and then sealed in a glove bag under argon atmosphere. The heating rate was 1 °C/min.

2.4. Electrochemistry

The Mo_6S_8 material used for the electrochemical experiments was prepared by copper extraction (leaching) from the synthetic products with intended composition $Cu_2Mo_6S_8$. The leaching procedure is described elsewhere [27]. The composite electrodes are 80% active mass, 10% carbon black, and 10% polyvinylidene fluoride (PVdF) pasted on a stainless steel mesh with mass load of approximately 4–7 mg/cm^2. Using slow scanning rate cyclic voltammetry, the electrodes were cycled in standard three-electrode cells comprising strips of Mg foil as counter and reference electrodes, and 0.25 M $Mg(AlCl_2BuEt)_2$ as complex electrolyte solution in Tetrahydrofuran (THF) (see reference [6] for the relevant experimental details). The scan rate was 0.05 mV/s using a VMP2 multichannel potentiostate (Princeton Applied Research) controlled by EC-Lab software.

3. Results and discussion

3.1. Combustion as a promising method to synthesize cluster compounds

Fig. 3 presents the results of quantitative XRD analysis for the synthetic products obtained by SHS technique (frontal combustion mode). As can be seen, for all the systems studied herein, the main products are the desirable Chevrel phases, while the by-products are mostly molybdenum chalcogenides: MoT_2 (T=S, Se) and Mo_2S_3 in the sulfur-containing systems. The undesirable formation of layered MoT_2 is really difficult to avoid, even in the traditional solid-state synthesis of Chevrel phases. To decrease the MoT_2 by-product in the ternary M–Mo–T reactions, it is commonly recommended [11] to increase the homogeneity of the initial mixture, which depends mostly on the particle size.

Particle size is known as one of the most important parameters in the combustion process. Thus, in the Cu–Mo–S synthesis, we replaced the copper precursor with the round-shaped (beads) morphology (particle surface of 0.21 m^2/g) by dendrite-shaped Cu particles (0.8 m^2/g) (Fig. 1(b) and (a), respectively). This resulted in the significant increase in the amount of the desirable Chevrel phase from ~36 to 86%. The content of non-reacted Mo in the synthesis products decreased respectively from 47 to 3%. In contrast, the effect of size for two different Mo precursors (Fig. 1(c) and (d)) on the synthetic results was negligible. A typical morphology of the SHS product, $Cu_2Mo_6S_8$, is presented in Fig. 4.

Our attempt to prepare $MnMo_6S_8$ from the element mixture was unsuccessful. The most obvious reason is the too big size of the Mn particles ranging from 8 to 35 μm. However, similar results were found for the fine material in the ternary Mn–Fe–S mixture [22], where the flame speed decreased with the Mn content. Hence, it is quite probable that the high heat release (T_{ad} for the Mn–S system is about 3000 K) is associated with too fast melting of the particles and their coalescence in the combustion front [28]. To avoid this problem, the green mixture should be diluted by an inert or less reactive material. In fact, by replacing Mn in the green mixture with fine MnS particles (1–2 μm), we obtained a Chevrel phase yield of 72% (Fig. 3). For the Pb-containing systems, in order to improve the combustion reaction, the green elemental mixture was diluted with the products of the previous synthesis (with lower yield of the Chevrel phase).

It is clear that the partial pressure of the sulfur or selenide vapors is one of the crucial parameters in the chalcogenides synthesis. As a result, for almost all the materials under study, the combustion was more successful in the argon atmosphere (high vapor pressure) than in vacuum. The exception is the Mn–Mo–S system, where the best results were achieved for the mixtures sealed under vacuum, probably due to the use of the MnS sulfide instead of the elements. We verified also the effect of the initial temperature on the combustion reaction. For all the ternary systems, increasing the initial temperature from 800 to 1500 °C (using Bunsen burner instead of the temperature controlled furnace) led to higher Chevrel phase yield. In contrast, for the binary Mo–Se system, the lower temperature favored the stable combustion.

These preliminary studies confirmed that Chevrel phases can be prepared by SHS, but also showed that each M–Mo–T system required individual optimization of all synthetic parameters like particle size of reactants, composition of the green mixture,

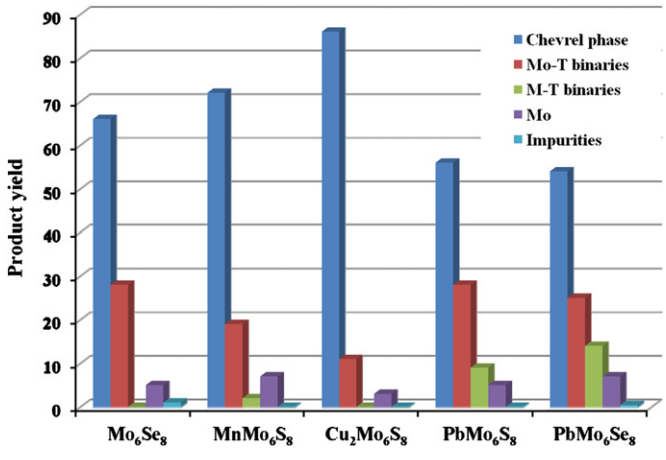

Fig. 3. The phase compositions of the SHS products (concluded from their Rietveld X-ray analysis).

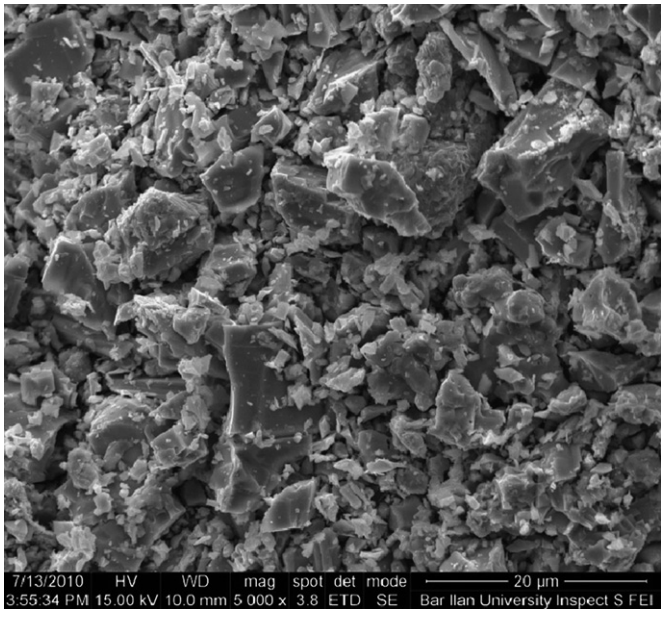

Fig. 4. A scanning electron microscopy image of the SHS product, $Cu_2Mo_6S_8$. Particle size is 4–12 μm.

combustion atmosphere and pressure, initial temperature, etc. We concentrated further in $Cu_2Mo_6S_8$, as the most important material for Mg rechargeable batteries, attempting to obtain both very fast synthesis and high yield.

3.2. Mechanisms of the $Cu_2Mo_6S_8$ synthesis

In the previous works, the main research interest in the Cu–Mo–S system was focused on the crystal structure of Chevrel phases $Cu_xMo_6S_8$ and its changes with temperature and copper amount [1, 2, 29]. Less is known about the mechanism of the phase formation upon the solid-state synthesis. Flukiger et al. [30] showed that the phase stability limits of the compound (melting point 1750 ± 30 °C for $x=2$) varied strongly with temperature: $1.2 \le x \le 3$ at 1500 °C and $1.8 \le x \le 4$ at 850 °C. The material with $x < 1.8$ obtained at high temperatures transformed upon cooling into the mixture of $Cu_{1.8}Mo_6S_8$, Mo_2S_3 and Mo. According to Huang et al. [31], the stable synthetic products in this system at 500 °C are CuS, Cu_2S and MoS_2, while Mo_2S_3 and Chevrel phase $Cu_2Mo_6S_8$ form above 600 °C. Below we show that, in order to understand the combustion mechanism, it is necessary to study the phase relations at relatively low temperatures (< 500 °C).

The combustion process for the Cu–Mo–S system can be presented as two separate reactions between binaries:

$$Cu + S \rightarrow CuS \quad (1)$$

$$Mo + 2S \rightarrow MoS_2 \quad (2)$$

From the stoichiometry of the initial mixture (Cu:Mo:S= 1:3:4), it is clear that the sulfur amount is insufficient to complete both of them, thus, the reactions can be regarded as competitive. The heat release of the first reaction should be essentially lower because of the difference in the flame temperatures T_{ad}: about 1000 and 2400 K for Cu–S and Mo–S systems, respectively [20] (melting points: 507 °C for CuS [32] and 2375 °C for MoS_2 [2]).

The subsequent reactions for both of the products should result in the formation of desirable Chevrel phase, e.g.,:

$$2CuS + 6Mo + 6S \rightarrow Cu_2Mo_6S_8 \quad (3)$$

$$4MoS_2 + 2Mo + 2Cu \rightarrow Cu_2Mo_6S_8 \quad (4)$$

$$2CuS + 3MoS_2 + 3Mo \rightarrow Cu_2Mo_6S_8 \quad (5)$$

However, according to the phase diagrams known for the binary and ternary systems [2, 30–32], the reactions (1)–(5) may be significantly more complex because of a possible variety of the synthetic products: Cu_xS (x changes from 1 to 1.2 and from 1.74 to 2) [29], Mo_2S_3 [2] and $Cu_xMo_6S_8$ with x ranged from 1.8 to 3.6 [1, 2, 30]. For instance, X-ray Rietveld analysis of the synthetic product obtained by frontal combustion (Fig. 5) showed 86% of desirable Chevrel phases with different unit cell parameters (and, respectively, with different Cu content), 10 MoS_2, 3 Mo and 1% Mo_2S_3. To account the non-homogeneous distribution of Cu in the Chevrel phases, the model of apparent strain was used in the refinement for the main phase 1 (54%). However, this model was insufficient to describe properly the X-ray diffraction profile of the synthesized product due to the relatively large difference in the unit cell parameters of the four phases listed in Fig. 5 (The inset in Fig. 5 shows the asymmetry of two diffraction peaks (1 1 0) and (0 1 2)). It is interesting to note that similar non-homogeneity in the phase composition was found previously in our Synchrotron studies of the synthetic products obtained by common solid state synthesis [29].

To clarify the synthetic mechanism, we had to determine the formation temperature of the main phases in reactions (1)–(5). For this, we used a combination of electron microscopy and X-ray powder diffraction for the products obtained at different temperatures by gradual heating. It should be mentioned that the use of such products to rationalize an extremely fast SHS process has, a-priori, some limitations, because one can miss the existence of unstable intermediate phases. In spite of these limitations, our analysis allowed to study the key sequence in the formation of the main phases.

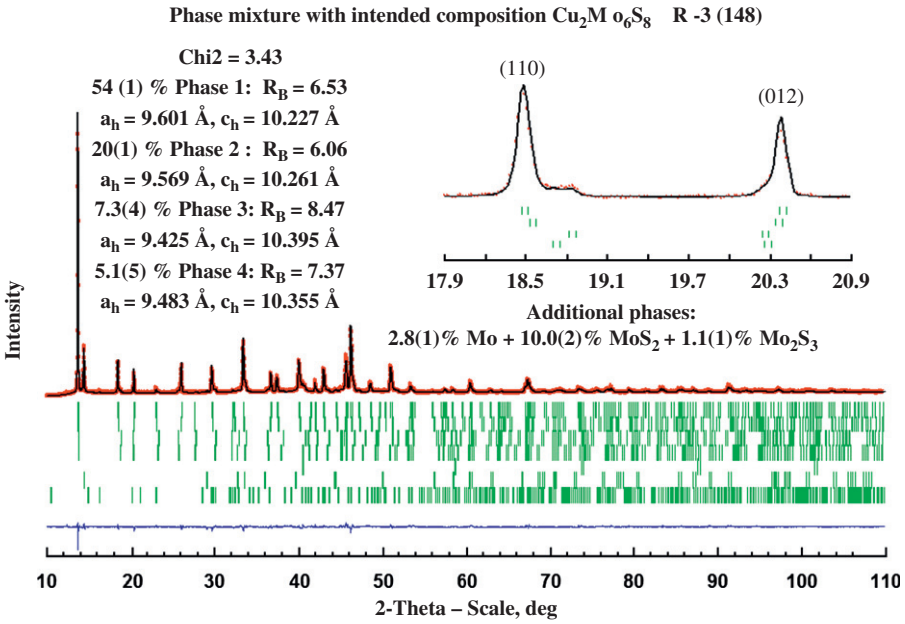

Fig. 5. A Rietveld X-ray diffraction profile of the SHS (frontal combustion mode) product with intended $Cu_2Mo_6S_8$ composition. The calculated 2θ values of the reflections (vertical bars) correspond to four Chevrel phases, $Cu_xMo_6S_8$ (which differ by the unit cell parameters), Mo, MoS_2, and Mo_2S_3 (top–down).

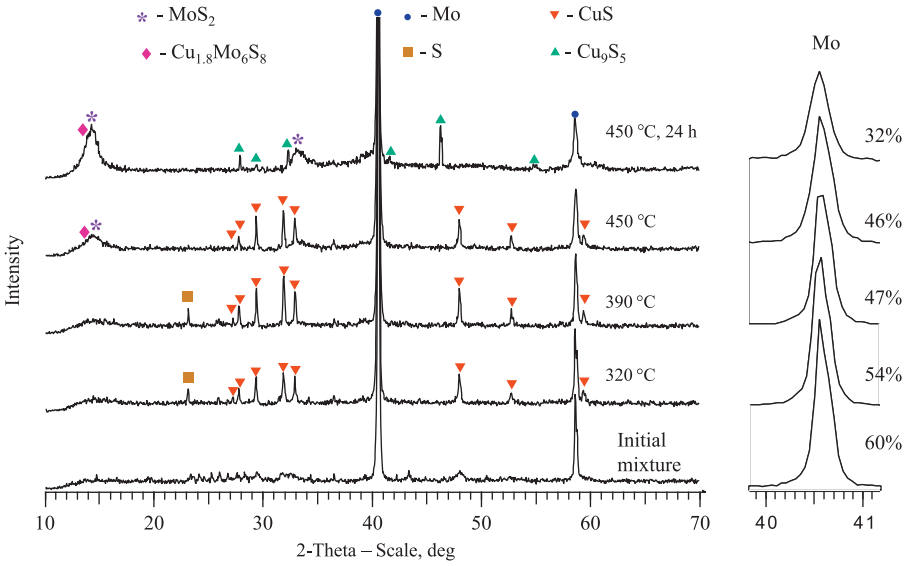

Fig. 6. XRD patterns of the initial Cu–Mo–S (1:3:4) mixture, the products of gradual heating up to 320, 390, 450 °C, and 24 h annealing at 450 °C.

It is well known [32, 33] that the ignition temperature T_{ign} of reaction (1) is very low: the Cu_xS formation was observed even during storage or pressing of the Cu–S mixtures at room temperature. In contrast, T_{ign} of reaction (2) is much higher: 584 ± 10 °C [20]. In spite of the relatively low heat release of the first combustion reaction (1), it might be sufficient to initiate the second combustion reaction (2) or/and the Mo diffusion into CuS with formation of Chevrel phase, $Cu_xMo_6S_8$.

Fig. 6 compares the XRD patterns of initial Cu–Mo–S mixture and the products of its heating in the temperature range 320 – 450 °C. In addition to CuS, the XRD pattern of the product heat-treated up to 320 °C showed a slight decrease of the Mo peak and the appearance of the sulfur peak related to its crystallization from the amorphous state. Heating from 320 to 450 °C did not result in appearance of new peaks of well-defined crystalline phase, but only in a broad diffraction peak around $2\theta = 14°$, which might be related to formation of quasi-amorphous phases with binary Mo–S or/and ternary Mo–Cu–S composition. Such suggestion agrees with the gradual decrease of the Mo amount with heating from 60% (weight) in the initial mixture to ~32% after its annealing (24 h) at 450 °C. The diffraction peak of unreacted sulfur disappeared only after heating up to 450 °C, i.e., the MoS_2 formation in the system under study seemed to begin between 390 and 450 °C. Appearance of the Cu_2S peak instead of the peak of CuS on the XRD pattern obtained after annealing at 450 °C provides additional evidence of the ternary system over-heating as compared to the reactions in the binary systems (according to the binary phase diagram [32], Cu_2S should appear only after melting of CuS at 507 °C and its transformation into Cu_2S above this temperature: $2CuS \rightarrow Cu_2S + S$). As the CuS melting is accompanied by sulfur delivery, it should initiate additional MoS_2 formation and the corresponding heat release.

Fig. 7 presents differential scanning calorimetry curve for the Cu–Mo–S (1:3:4) mixture in the temperature range 40–450 °C. Two endothermic peaks above 95 °C are related to the phase transitions of sulfur, including its melting at ~117 °C. The exothermic peak in the temperature range of 330–370 °C can be assigned to formation of CuS (such interpretation seems to be in contradiction with the XRD data, but, as was shown by Blachnik et al. [32], the position of the thermal peak related to the Cu_xS formation is affected greatly by the sample preparation). The second exothermic process begins above 400 °C. According to the data of X-ray diffraction (Fig. 6) and electron microscopy (see below), this peak should be related to

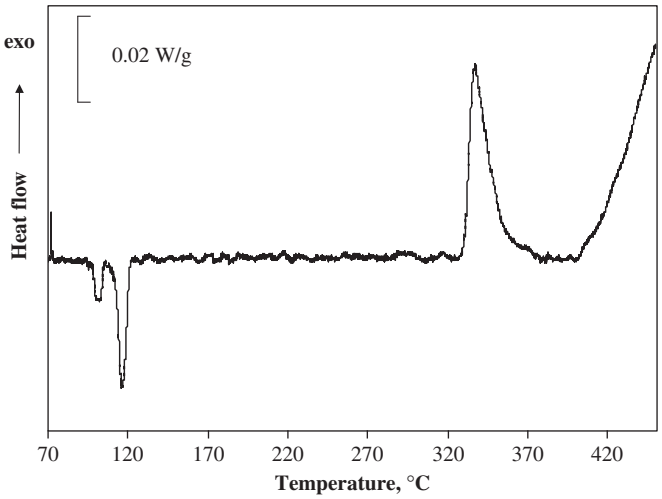

Fig. 7. Differential scanning calorimetry curve for the Cu–Mo–S (1:3:4) mixture in the temperature range 40–450 °C.

formation of new phases, MoS_2 and $Cu_xMo_6S_8$, as well as to transformation of CuS to Cu_2S.

Figs. 8 and 9 show the electron microscope images of the synthetic product obtained by gradual heating of the Cu–Mo–S (1:3:4) mixture up to 450 °C (without annealing). As can be seen, the presented data confirm the appearance of nano-crystalline MoS_2 and Chevrel phases, $Cu_xMo_6S_8$, at these low temperatures. Thus, the heat realized in the Cu–S combustion triggers the subsequent reactions, e.g., the combustion between Mo and S in the ternary mixture proceeds at essentially lower heating temperature than T_{ign} (584 °C) of the binary Mo–S mixture. Interestingly, similar formation of nano-crystalline Chevrel phase, $Cu_xMo_6Se_8$, was found previously [11] by TEM studies of the selenide Cu–Mo–Se mixture heat-treated at 550 °C.

The results presented testify that nucleation of the desirable Chevrel phase and of the MoS_2 impurity began at similar low temperatures (< 450 °C). These results also showed that the MoS_2 formation upon heating in this system is unavoidable. Moreover, in the case of SHS, the MoS_2 formation was the main source of heat needed for stable combustion. To minimize the MoS_2

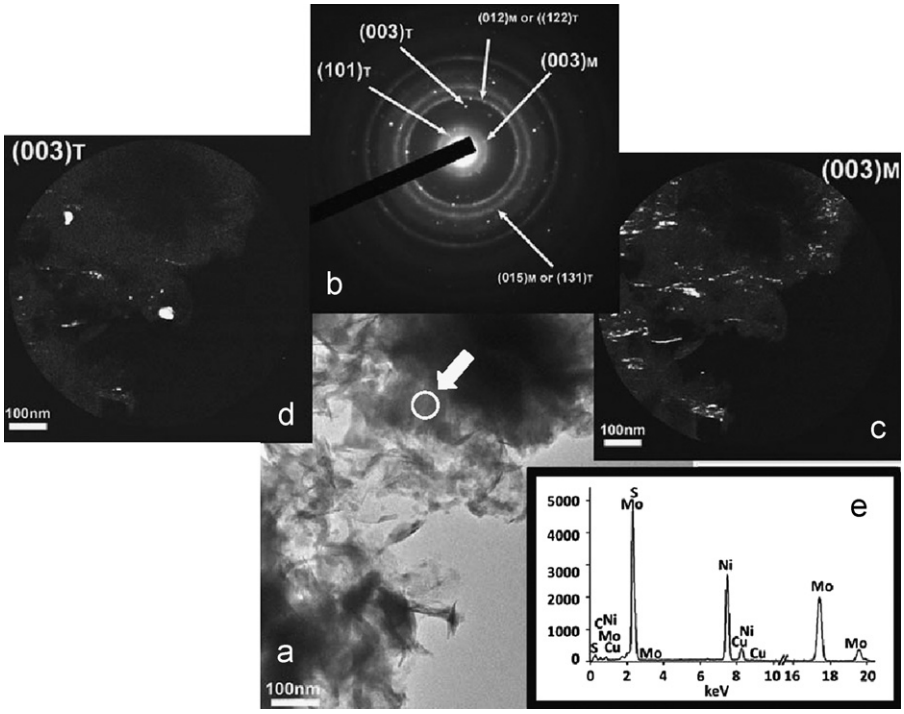

Fig. 8. Transmission electron micrographs of the representative nano-particles of the synthetic product obtained by gradual heating of the Cu–Mo–S (1:3:4) mixture up to 450 °C: (a) Bright field (BF) image. (b) SAED taken from an area of 700 nm, shows the reflections of all the nano-particles presented in the analyzed area. As expected from polycrystalline nano-particles, the SAED is mainly a ring diffraction pattern, and reflections belonging to different zone axis will also appear in the diffraction pattern. Marked are the characteristic reflections for the layered MoS_2 (M) and the Chevrel phase, $Cu_2Mo_6S_8$ (T). The indexing was performed with the following unit cell parameters: a=3.16 Å, c=18.45 Å for MoS_2 (pdf file 000471519) and a=9.73 Å, c=10.2 Å for Chevrel phase. (c) and (d) Dark field (DF) images taken using the characteristic reflection (0 0 3)M for MoS_2 (c) and (0 0 3)T for the Chevrel phase (d). Hence, the bright sports (the crystalline particles) display the spatial distributions of MoS_2 (c) and Chevrel phase, $Cu_xMo_6S_8$ (d). e – EDS spectrum recorded with a 35 nm electron probe from these nano-particles (marked by the white arrow), showing characteristic peaks of Mo, Cu and S. The Ni peak is from the supporting grid.

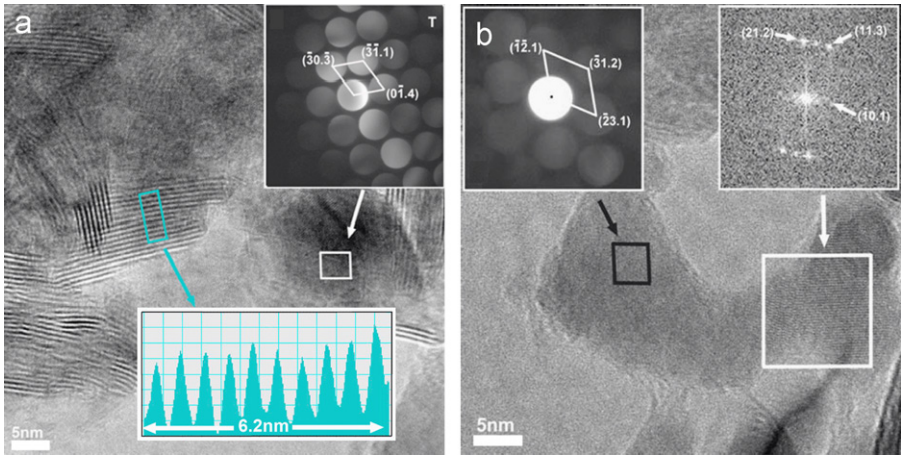

Fig. 9. Two high-resolution transmission electron microscopy images of the synthetic product obtained by gradual heating of the Cu–Mo–S (1:3:4) mixture up to 450 °C. The nano-beam diffraction (the upper insert in (a) and the left upper insert in (b)) and the Fourier transform pattern (the right upper insert in (b)) are related to nano-crystalline Chevrel phase, $Cu_xMo_6S_8$. The d-spacing of 0.62 nm (atomic planes in the blue rectangular) can be assigned to the 003 planes of MoS_2 (The lower insert with the line scan profile presents the 10-spacing from this area).

amount in the final product we have to modify the synthetic conditions.

3.3. *Bulk combustion for $Cu_2Mo_6S_8$*

In the conventional synthesis, the kinetics of the phase growth and crystallization are limited by slow solid-state diffusion. Thus, preparation of the pure Chevrel phases can be successfully achieved only upon long annealing at high temperatures. For SHS, the success of the process depends mostly on the energetic parameters. The presence of phases such as the Mo sulfides and the unreacted Mo in the final product showed the incompleteness of the Chevrel phase synthesis, which may be related to insufficient heating or inhomogeneity of the heat distribution in the combustion reactor.

To improve the energetic conditions for this reaction, we changed the combustion mode from the frontal wave to the thermal explosion: The Swagelok stainless-steel vessel with initial mixture (2 g) was put into the hot furnace (1000 °C) for 2 and 10 min. Due to the replacement of quartz tube by a

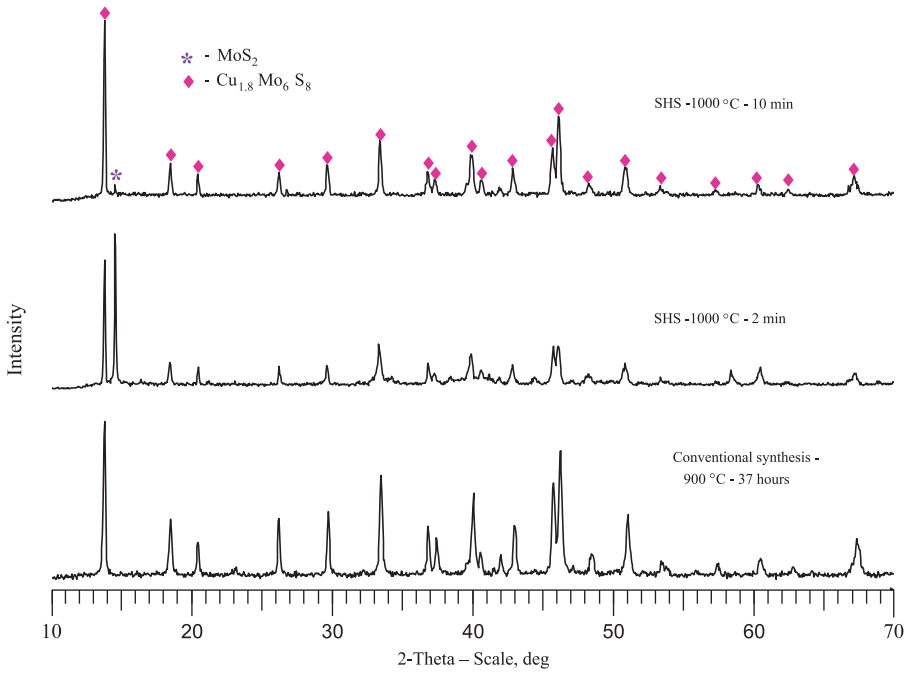

Fig. 10. XRD patterns for the products of the conventional synthesis (20 h of heating up to 900 °C+17 h of annealing at this temperature) and thermal explosion (2 and 10 min at 1000 °C).

Swagelock vessel, the ratio between reactant and total reactor volumes was changed from 1:10 to 1:2. To increase the partial pressure of the sulfur vapors and to avoid possible sulfur loss caused by its reaction with the stainless steel, we added an extra amount of sulfur to the initial mixture ($Cu_2Mo_6S_{8.5}$ stoichiometry). This extra sulfur also favored reaction (2) with high heat release.

Fig. 10 compares the XRD patterns for the products of the conventional synthesis (20 h of heating up to 900 °C+17 h of annealing at this temperature) [13] and thermal explosion (2 and 10 min at 1000 °C for 2 g of reactants). As can be seen, 2 min of heating is not sufficient to complete the Chevrel phases synthesis, but after 10 min the phase composition of the product is identical to the conventional one. The qualitative XRD analysis showed that, with improved SHS technique, we succeeded to increase the yield to 96%. Similar results were obtained for larger Swagelok vessel with 5 g of reactants (with the ratio between reactant and total reactor volumes being the same, 1:2), but in this case 20 min at 1000 °C were needed to complete the synthesis.

3.4. Electrochemical activity of the SHS product

The Cu-containing Chevrel phases obtained by thermal explosion and conventional solid-state reaction were leached (Cu-extraction) to Mo_6S_8 phases and tested as cathode materials in prototype rechargeable Mg batteries (three electrodes cells, as detailed in the experimental section). Their steady-state cyclic voltammetric response is presented in Fig. 11. The expected electrochemical behavior was found for both products, which indicated reversible insertion of two Mg^{2+} ions per Mo_6S_8. Thus, $Cu_2Mo_6S_8$ prepared by the new SHS route holds the promise to successfully be used as active cathode material in rechargeable Mg batteries.

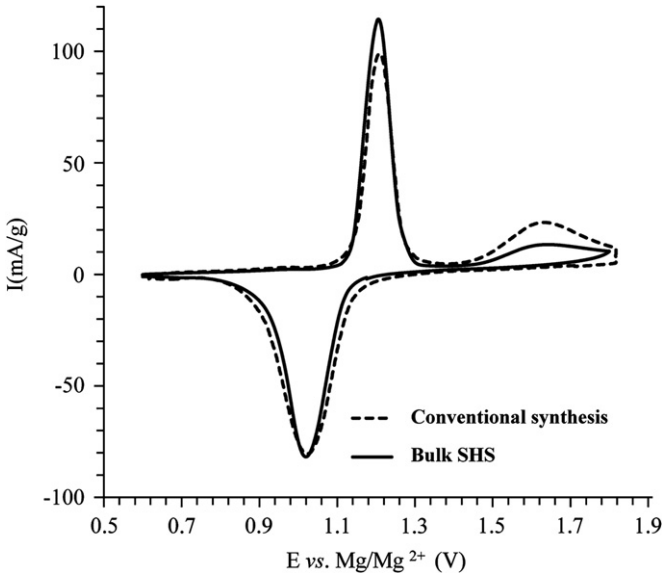

Fig. 11. Cyclic voltammetry curves (plot of current *I* vs. potential *E*) for reversible Mg-ions insertion into composite Mo_6S_8 cathodes (produced by SHS and conventional solid-state methods as indicated) measured in prototype Mg batteries (Mg strip counter & reference electrodes, 0.25 M $Mg(AlCl_2BuEt)_2$ complex electrolyte solution in THF at a scan rate of 0.05 mV/s.

4. Conclusions

We described new fast synthesis approaches to form Chevrel phases with high yield (96% for $Cu_2Mo_6S_8$). The synthesis duration was a few minutes compared to the many hours or even days of the existing techniques. Chemical reactions and mechanisms for the Cu–Mo–S system were extrapolated from combined electron microscopy and X-ray diffraction, which revealed Chevrel phase formation at temperatures as low as 450 °C. The electrochemical behavior of $Cu_2Mo_6S_8$ obtained by combustion was similar to that of the conventional product. Thus, self-propagating high-temperature synthesis can be considered as a very promising alternative method for the production of cluster-containing chalcogenides.

References

[1] K. Yvon, in: E. Kaldis (Ed.), Current Topics in Material Science, Vol. 3, North-Holland, Amsterdam, 1979, pp. 53–129.
[2] Ø. Fisher, M.B. Maple, Topics in Current Physics: Superconductivity in Ternary Compounds I, Springer-Verlag, Berlin, 1982.
[3] T. Caillat, J.P. Fleurial, G.J. Snyder, Solid State Sci. 1 (1999) 535–544.
[4] N. Alonso-Vante, in: W. Vielstich, A. Lamm, H. Gasteiger (Eds.), Handbook of Fuel Cells, vol. 2, Wiley, Chichester, 2003, pp. 534–543.
[5] E. Levi, G. Gershinsky, D. Aurbach, O. Isnard, G. Ceder, Chem. Mater. 21 (2009) 1390–1399.
[6] D. Aurbach, Z. Lu, A. Schechter, Y. Gofer, H. Gizbar, R. Turgeman, Y. Cohen, M. Moskovich, E. Levi, Nature 407 (2000) 724–727.
[7] E. Levi, Y. Gofer, D. Aurbach, Chem. Mater. 22 (2010) 860–868.
[8] S. Seghir, C. Boulanger, S. Diliberto, J.M. Lecuire, M. Potel, O. Merdrignac-Conanec, Electrochem. Commun. 10 (2008) 1505–1508.
[9] R. Chevrel, M. Sergent, J. Prigent, J. Solid State Chem. 3 (1971) 515–519.
[10] S. Even-Boudjada, L. Burel, R. Chevrel, M. Sergent, Mater. Res. Bull. 33 (1998) 419–431.
[11] R. Schneidmiller, A. Bentley, M.D. Hornbostel, D.C. Johnson, J. Am. Chem. Soc. 121 (1999) 3142–3149.
[12] M. Rabiller-Baudry, M. Sergent, R. Chevrel, Mater. Res. Bull. 26 (1991) 519–526.
[13] D. Aurbach, G.S. Suresh, E. Levi, A. Mitelman, O. Mizrahi, O. Chusid, M. Brunelli, Adv. Mater. 19 (2007) 4260–4267.
[14] E. Lancry, E. Levi, A. Mitelman, S. Malovany, D. Aurbach, J. Solid State Chem. 179 (2006) 1879–1882.
[15] A.G. Merzhanov, I.P. Borovinskaya, Dokl. Akad. Nauk SSSR 204 (1972) 366–369.
[16] A.G. Merzhanov, I.P. Borovinskaya, Combust. Sci. Technol. 10 (1975) 195–201.
[17] Z.A. Munir, U. Anselmi-Tamburini, Mat. Sci. Rep. 3 (1989) 279–365.
[18] J.J. Moore, H.J. Feng, Prog. Mater Sci. 39 (1995) 243–273.
[19] A.G. Merzhanov, J. Mater. Chem. 14 (2004) 1779–1786.
[20] S. Goroshin, A. Mizera, D. Frost, J.H.S. Lee, Proc. Combust. Inst. 26 (1996) 1883–1889.
[21] S.V. Goroshin, J.H.S. Lee, D.L. Frost, Twenty-Fifth Symposium (International) on Combustion, The Combustion Institute, Pittsburgh, 1994, pp. 1651–1657.
[22] S. Goroshin, L. Camargo, J.H.S. Lee, Proc. Combust. Inst. 30 (2005) 2561–2568.
[23] V.L. Kalikhman, A.A. Golubnichaya, E.P. Gladchenko, V.K. Prokudina, L.P. Schepinova, Sov. Powder Metall. 10 (1982) 56–59.
[24] H.M. Rietveld, J. Appl. Crystallogr. 2 (1969) 65–71.
[25] J.R. Carjaval, Physica B 192 (1993) 55–69.
[26] L.B. McCusker, R.B. Von Dreele, D.E. Cox, D. Louer, P.J. Scardi, Appl. Crystallogr. 32 (1999) 36–50.
[27] E. Lancry, E. Levi, Y. Gofer, M. Levi, G. Salitra, D. Aurbach, Chem. Mater. 16 (2004) 2832–2838.
[28] I.G. Cano, I.P. Borovinskaya, M.A. Rodriguez, V.V. Grachev, J. Am. Ceram. Soc. 85 (2002) 2209–2211.
[29] E. Levi, A. Mitelman, D. Aurbach, M. Brunelli, Chem. Mater. 19 (2007) 5131–5142.
[30] R. Flukiger, R. Baillif, J. Muller, K. Yvon, J. Less-Common Met. 72 (1980) 193–204.
[31] D. Huang, L.L.Y. Chang, C.R. Knowles, J. Less-Common Met. 163 (1990) 281–286.
[32] R. Blachnik, A. Muller, Thermochim. Acta 361 (2000) 31–52.
[33] H. Wada, K. Takada, T. Sasaki, Solid State Ionics 172 (2004) 421–424.